Large Eddy Simulation of Flame Acceleration in an Obstructed Channel

Craig Johansen and Gaby Ciccarelli

Department of Mechanical and Materials Engineering, Queen's University
Kingston, Ontario, Canada

1 Introduction

The study of flame acceleration in an obstructed channel has applications ranging from explosion safety to high speed propulsion [1, 2]. From the onset of spark ignition at the closed end of a channel, the development of the flow field in the unburned gas ahead of the flame has a large influence on the rate of flame acceleration leading up to DDT [3]. In a previous study, fence type obstacles mounted on the top and bottom surfaces of a square cross-section channel were found to distort the unburned gas flow field [4]. The generation of a shear layer from the obstacle tips results in the production of turbulence, which increases the total transport of mass, momentum, and energy in the flow. A feed-back loop is formed between the volumetric burning rate and the unburned gas velocity, which leads to flame acceleration. At the later stages of flame acceleration just prior to DDT, shock-flame interactions become the dominant mechanism responsible for flame acceleration [1]. In this study, however, attention is focused on the initial stages of flame acceleration where shock-flame interactions and other compressibility effects are not important.

Recent numerical simulations of flame propagation in obstructed channels have provided insight into the mechanisms responsible for flame acceleration. Gamezo et al. [5] simulated flame acceleration from spark ignition up to the initiation and propagation of a detonation wave. Although global parameters such as the DDT run-up distance agree well with experimental values, the simulations ignored the effects of turbulence on the overall process. Bychkov et al. [6] performed simulations of the initial stages of flame acceleration in an obstructed channel prior to DDT for the purpose of developing an analytical model to predict changes in the flame speed. Similarly, the turbulence field was under-resolved and no turbulence model was used. A large eddy simulation (LES) focused on the development of the turbulence field in the unburned gas ahead of the flame was performed by Johansen and Ciccarelli [7]. It was found that the unsteady development of flow structures ahead of the flame is closely coupled to the evolution of the flame shape that is observed experimentally. Building on that work, this study aims to further understand the interaction between the flame surface and the turbulence field by modeling flame propagation directly using a flame surface density combustion model with LES. Predictions of the flame shape development, flame-tip velocity, and flame area are compared to an experimental dataset [4].

Correspondence to: johansen@me.queensu.ca

2 Simulation Setup

A low-Mach number formulation of the compressible filtered governing equations were solved [8, 9]. The subgrid viscosity is calculated from the dynamic Smagorinsky-Lilly model [10, 11]. A progress variable, $\tilde{c}$, is used to track the distribution of the unburned ($\tilde{c}$ = 0) and burned gas ($\tilde{c}$ = 1). The filtered reaction rate and the molecular diffusion of $\tilde{c}$ are approximated using an algebraic flame surface density combustion model developed by Boger et al. [12]:

$$\frac{\partial}{\partial x_i}\left(\bar{\rho} D \frac{\partial \tilde{c}}{\partial x_i}\right) + \overline{\dot{w}_c} = \rho_u S_L \Sigma \tag{1}$$

where $\rho_u = 0.533$ kg/m^3 is the density of unburned stoichiometric methane-air gas mixture evaluated at the experimental initial conditions (P_i = 47 kPa, T_i = 293 K). From the chemical equilibrium software, Cantera, the laminar burning velocity is estimated to be 47 cm/s. The flame surface density, Σ, is approximated from the following relationship:

$$\Sigma = 4K\tilde{c}\left(1-\tilde{c}\right)/\Delta \tag{2}$$

Based on experimental flame-tip speed measurements, the subgrid wrinkling constant was determined empirically to be K = 0.27, which falls within the range of reported values from Boger et al. [12]. In these simulations, the filter size is equivalent to the node spacing, Δ. The governing equations were solved at second order accuracy using the segregated pressure-based solver of the commercial computational fluid dynamics software, ANSYS Fluent v.6.3. The computational domain and boundary conditions, shown in Fig. 1, correspond to one-quarter of the channel volume spanning roughly two obstacle pairs downstream of the ignition point.

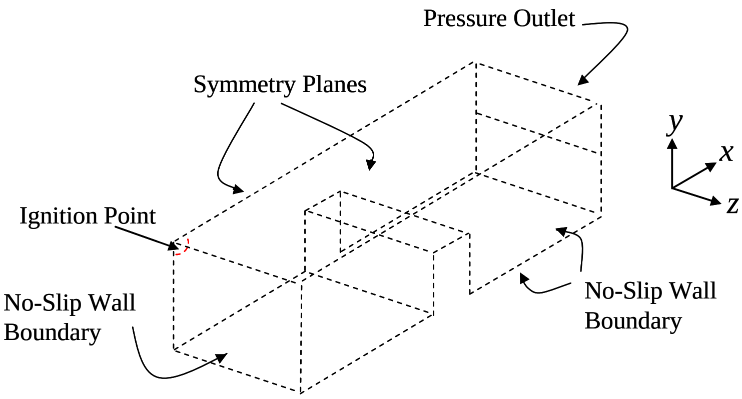

Figure 1: Computational domain and boundary conditions. BR = 0.5, W/H = 0.5, L/H = 2.8

The obstacle spacing is equal to the channel width (W) and height (H) of 7.62 cm. The length of the computational domain was varied from L/H = 2.8 to L/H = 10. The base grid has a node spacing of Δ = 0.6 mm, which corresponds to H/Δ = 127 and a total node count ranging from 1 million nodes (L/H = 2.8) to 5 million nodes (L/H = 10) in the entire domain. An extensive sensitivity study of the effects of grid spacing, domain shape, and temporal resolution are available in the literature [7,9]. The velocity, and progress variable in the computational domain were initially set U_i = 0 m/s, and $\tilde{c}_i$ = 0. The ignition source was positioned at the intersection of the end wall surface, the x-y symmetry plane, and the x-z symmetry plane. The initiation of the flame kernel was achieved through patching in the combustion products ($\tilde{c}$ = 1) into a hemispherical volume at the ignition point. The initial flame kernel radius was r_i = 6 mm. The pressure outlet was maintained at the initial pressure and temperature of the reactants.

3 Simulation Results

Figure 2 shows simulation predictions of the flame shape in both the *x-y* and *x-z* planes (refer to Fig. 1 for plane designation) compared to experimental schlieren images taken from reference [4]. The obstacle blockage ratio (BR) at this condition is 0.67. The simulation time, *t*, was adjusted by subtracting 3.38 ms from the simulations in order to properly synchronize to the experiment. At t = 0 ms, the simulated flame-tip position is not at x/H = 0 due to the flame surface initialization method. In addition, in the experiment there is significant heat transfer between the flame surface and spark plug shortly after ignition. The simulation does not include the flame development at the spark plug nor does it include heat transfer to the wall boundaries. After the initial modification to the simulation time, the experiment and simulation remained roughly synchronized over several obstacle pairs (Fig. 2). Since the schlieren images provide the integrated effect of the density gradients over the entire channel width (W/H = 1), the simulation results are presented as a projected three-dimensional iso-surface ($\tilde{c}$ = 0.5) onto each of the respective planes. The total flame surface was created by reflecting the computational domain over each of the symmetry planes shown in Fig. 1.

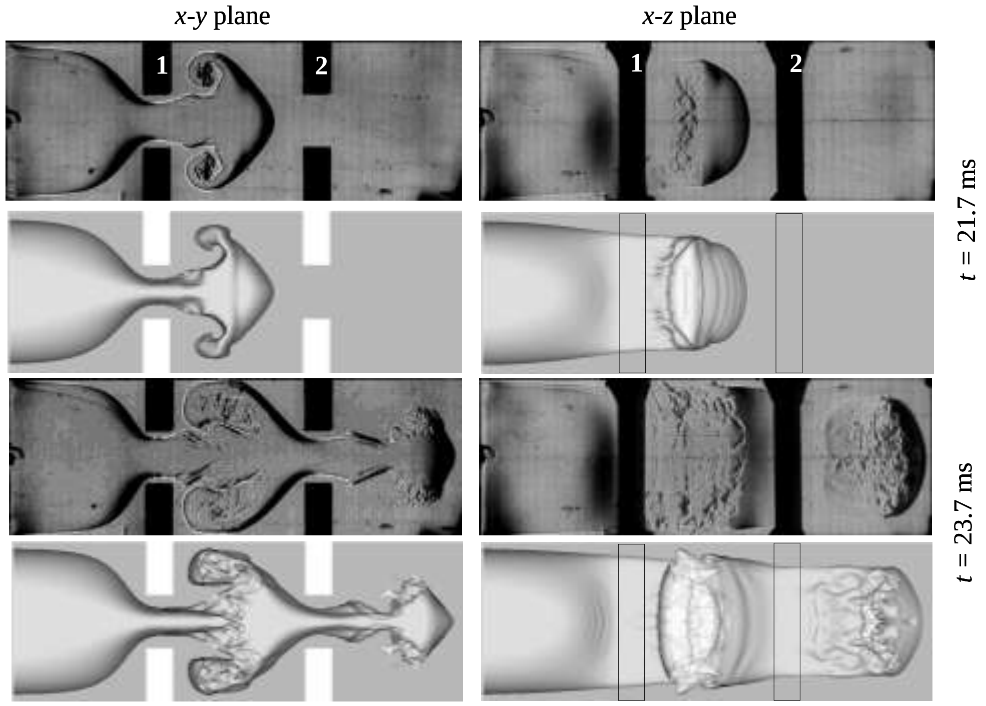

Figure 2: Simulation predictions of flame shape (bottom row, $\tilde{c}$ = 0.5 iso-surface) compared to schlieren images (top row). Both *x-y* and *x-z* planes shown. *BR* = 0.67 and obstacle #s shown in white.

The simulations accurately predict the overall flame shape, including many of the smaller features observed in the schlieren images. The roll-up of the vortex downstream of obstacle #1, for example, is a feature predicted in the simulations. The extent of the entrainment of the flame surface into the vortex roll-up, however, is smaller in the simulations compared to the schlieren images. In both the simulation and the experiment, the development of the shear layer downstream of obstacle #2 results in an elongated flame shape. The flame propagates along the core and then "mushrooms" near the end of the domain before the third obstacle. The destabilization of the vortex core at 23.7 ms is well predicted in terms of the extent of the flame wrinkling observed in the x-z plane. Figure 3 shows a quantitative comparison between the simulation and the experiment of the axial variation of the centerline flame-tip velocity and flame area as a function of the flame tip position. Accurate predictions of the oscillations in flame-tip velocity from the contraction and expansion of the unburned gas gives confidence to the simulations. The flame area, however, is slightly under-predicted in the simulations. This is confirmed by examining Fig. 2, where the lateral flame surface is much closer to the channel top and bottom walls in the schlieren images compared to the simulations in both the *x-y* and *x-z* planes. A lower simulated flame area is expected due to the filtering process of LES, which acts to smooth out the smaller scales.

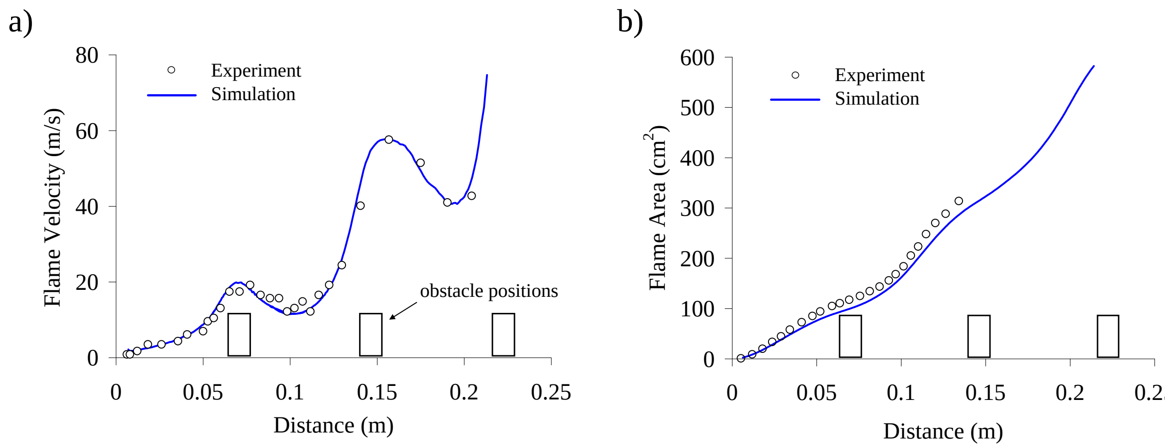

Figure 3: Simulation predictions of the centerline flame velocity (a) and the flame area (b). BR = 0.67, L/H = 5.8, and H/Δ = 127.

Figure 4 shows the distribution of vorticity, stream-traces, and the projection of the translucent $\tilde{c}$ = 0.5 iso-surface for two different simulation times. Note that these images were constructed using the planes of symmetry shown in Fig. 1. Strong vorticity is present along the lateral flame surface at each obstacle where a strong velocity gradient exists. As expected the intensity of the vorticity is stronger at obstacle #2 compared to obstacle #1. Also evident in this image is the train of small secondary vortices that are shed from obstacle #2. The "mushrooming" effect observed in the schlieren images (Fig. 2, t = 23.7 ms) is due to the convection of the flame-tip along the shear layer, which follows the shape of the large recirculation zone. Expansion of the stream-traces caused by the rotational velocity of the vortex occurrs near the downstream side of the recirculation zone. Near the upstream side of the recirculation zone, stream-traces are roughly parallel in the horizontal direction. Since the unburned gas velocity magnitude is lower in the recirculation zones compared to the core flow, the lateral flame surface is more susceptible to distortions from lower strength vortices in the recirculation zone.

A diamond shaped feature, which appears just upstream of the mushroom shape, (Fig. 2, t = 23.7 ms, *x-y* plane) is observed in the experiment and predicted in the simulations. This phenomenon is also due to the development of the recirculation zones. In Fig. 4 (t = 23.7 ms), stream-traces expand and then contract immediately downstream of the second obstacle, which coincides with the formation of a small secondary vortex at the obstacle's trailing edge. For example, at t = 23.2 ms, the flame surface slowly expands near the flame-tip due to the formation of the main recirculation zone. Only small deformations exist along the lateral edge of the flame surface at this time. At t = 23.7 ms, the center of the main vortex associated with the recirculation zone convects downstream and a small secondary vortex forms at the obstacle trailing edge. This augments the stream-traces toward the channel surfaces and the flame shape propagates accordingly in the transverse direction. The stream-traces then redirect back towards the channel centerline as the velocity associated with the upstream side of the main recirculation zone points towards the channel centerline.

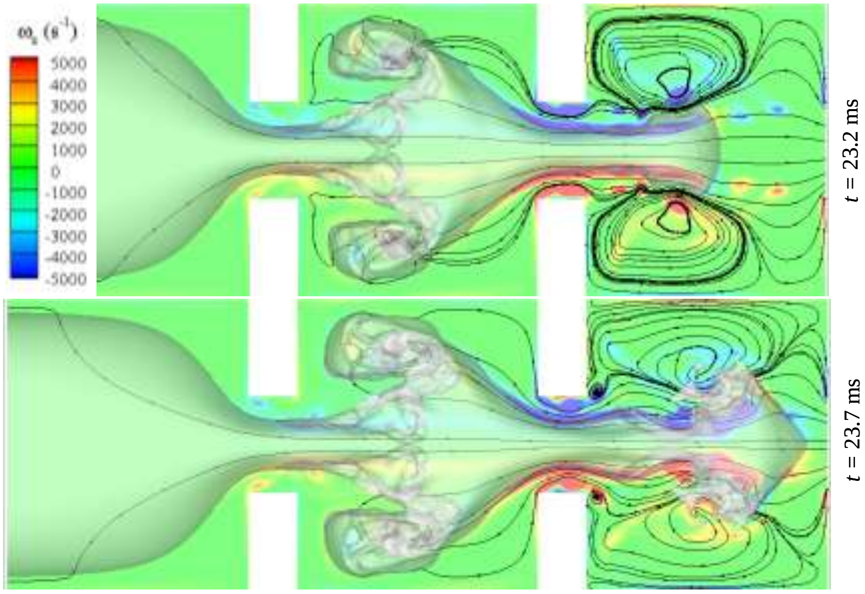

Figure 4: Distribution of vorticity for flame development after second obstacle. Stream-traces and $\tilde{c}$ = 0.5 iso-surface overlaid onto the vorticity contour. BR = 0.67.

4 Conclusions

Large eddy simulations of early-time flame propagation using a flame surface density combustion model have been undertaken and compared to experiment. The overall flame shape and large flame structures that are observed experimentally are predicted by the simulations. Quantitatively, the simulations accurately predict the experimental flame-tip velocity oscillations and the increase in flame area. Through analysis of the predicted solution, it was found that the flame shape becomes highly stretched in the stream-wise direction as small vortical structures form in the shear layer. The development of these small three-dimensional flow structures in the unburned gas results in a highly wrinkled transverse (or lateral) flame surface, which increases the bulk burning rate. The flame interaction with small recirculation zones at low flame speeds results in a relatively smooth roll-up of the flame surface. The "mushroom" shape of the flame-tip that is observed at higher flame speeds occurs due to flame interaction with a much larger recirculation zone. For these initial stages of flame acceleration, the main features in the flame shape evolve as a result of the continuing change in structure of the recirculation zones between obstacles.

References

[1] Ciccarelli, G and Dorofeev, S, (2008) Flame acceleration and transition to detonation in ducts. Prog. Energy. Combust. Sci. 34:499.

[2] Roy GD, Frolov, SM, Borisov, AA, and Netzer, DW, (2004) Pulsed detonation propulsion: challenges, current status, and future perspective, Prog. Energy. Combust. Sci. 30:545.

[3] Shchelkin, KI, (1940) Influence of tube roughness on the formation and detonation propagation in gas, J. Exp. Theor. Phys. 10:823.

[4] Johansen, CT, and Ciccarelli, G, (2009) Visualization of the unburned gas flow field ahead of an accelerating flame in an obstructed channel, 156:405.

[5] Gamezo, V, Takanobu, O, and Oran, ES, (2007) Numerical simulations of flame propagation and DDT in obstructed channels filled with hydrogen-air mixture, Proc. Combust. Inst. 31:2463.

[6] Bychkov, V, Valiev, D, and Eriksson, L, (2008) Physical mechanism of ultrafast flame acceleration, Phys. Rev. Lett. 101:1.

[7] Johansen, CT, and Ciccarellil, G, (2010) Numerical simulations of the flow field ahead of an accelerating flame in an obstructed channel, Combust. Theory. Modelling 14:235.

[8] Sagaut, P, (2009) Large eddy simulation for compressible flows, Springer-Verlag, New York.

[9] Johansen, C, (2009) Experimental and numerical investigation of flame acceleration in an obstructed channel, PhD Thesis Dissertation, Mechanical and Materials Engineering, Queen's University.

[10] Germano, M, Piomelli, U, Moin, P, and Cabot, WH, (1991) A dynamic subgrid-scale eddy-viscosity model, Phys. Fluids A3 1760.

[11] Lilly, DK, (1992) A proposed modification of the Germano subgrid-scale closure model, Phys. Fluids A4 633.

[12] Boger, M, Veynante, D, Boughanem, H, and Trouve, A, (1998) Direct numerical simulation analysis of flame surface density concept for large eddy simulation of turbulent premixed combustion, 27th Symp. Comb., Colorado.